RESEARCH ARTICLE

JCN RESEARCH IN SYSTEMS NEUROSCIENCE | THE JOURNAL OF COMPARATIVE NEUROLOGY   **WILEY**

Nitrergic neurons of the forepaw representation in the rat somatosensory and motor cortices: A quantitative study

Bárbara de Paula Pires Franco Guimaraes[1] | **Marco Rocha Curado**[2] |
Anaelli Aparecida Nogueira-Campos[3] | **Jean Christophe Houzel**[2] | **Ricardo Gattass**[1] (ORCID)

[1]Program of Neurobiology, Institute of Biophysics Carlos Chagas Filho, Federal University of Rio de Janeiro, Rio de Janeiro, Brazil

[2]Program of Morphological Science, Institute of Biomedical Science, Federal University of Rio de Janeiro, Rio de Janeiro, Brazil

[3]Laboratory of Cognitive Neurophysiology, Department of Physiology, Institute of Biological Science, Federal University of Juiz de Fora, Juiz de Fora, Minas Gerais, Brazil

Correspondence
Ricardo Gattass, Centro de Ciências da Saúde, Instituto de Biofísica Carlos Chagas Filho, Universidade Federal do Rio de Janeiro, Avenida Carlos Chagas Filho, 373, Bloco G - 2° andar- Sala G1-019, Cidade Universitária – Ilha do Fundão, 21941-902 Rio de Janeiro, Brazil.
Email: rgattass@gmail.com

Abstract

Nitrergic neurons (NNs) are inhibitory neurons capable of releasing nitric oxide (NO) that are labeled with nicotinamide adenine dinucleotide phosphate diaphorase histochemistry. The rat primary somatosensory (S1) and motor (M1) cortices are a favorable model to investigate NN populations by comparing their morphology, since these areas share the border of forepaw representation. The distribution of the Type I NN of the forepaw representation in the S1 and M1 cortices of the rat in different laminar compartments and the morphological parameters related to the cell body and dendritic arborization were measured and compared. We observed that the neuronal density in the S1 (130 NN/mm^3) was higher than the neuronal density in the M1 (119 NN/mm^3). Most NN neurons were multipolar (S1 with 58%; M1 with 69%), and a minority of the NN neurons were horizontal (S1 with 6%; M1 with 12%). NN found in S1 had a higher verticality index than NN found in M1, and no significant differences were observed for the other morphological parameters. We also demonstrated significant differences in most of the morphological parameters of the NN between different cortical compartments of S1 and M1. Our results indicate that the NN of the forepaw in S1 and M1 corresponds to a neuronal population, where the functionality is independent of the different types of sensory and motor processing. However, the morphological differences found between the cortical compartments of S1 and M1, as well as the higher density of NNs found in S1, indicate that the release of NO varies between the areas.

KEYWORDS
GABAergic neurons, interneurons, NADPH diaphorase, nitric oxide, primary motor cortex, primary somatosensory cortex

1 | INTRODUCTION

Nitric oxide (NO), the first gaseous neurotransmitter described in the nervous system, is involved in several physiological and pathological functions (Bredt & Snyder, 1992; Calabrese et al., 2007; Freire et al., 2012; Garthwaite, 2008; Moncada et al., 1991). In the brain, NO synthase (NOS) enzymes colocalize with nicotinamide adenine dinucleotide phosphate diaphorase (NADPHd) (Dawson et al., 1991;

Stuehr, 2004), providing a specific marker for NO-releasing neurons. NADPHd histochemistry reveals the presence of two types of NO-synthesizing neurons in the neuropil, which appears as a reactive background composed of neurites and very thin terminals (Franca et al., 2000). Type I neurons are intensely labeled and relatively sparse throughout the cortex. Although Type II neurons are more numerous than Type I neurons, Type II cells are smaller and display faint or unlabeled dendritic trees (Franca et al., 2000; Freire et al., 2004; Lüth et al., 1994; Yan et al., 1996; Yan & Garey, 1997).

Type I inhibitory neurons, referred to as nitrergic neurons (NNs), have been identified in several species studied, where they make up approximately 0.5–2% of total cortical neurons (Gabbott & Bacon, 1995). Although a few studies have investigated the nitrergic circuitry in somatosensory, motor, visual or auditory cortices, as well as in the hippocampus, cerebellum, striatum, and spinal cord (Franca et al., 2000; Freire et al., 2012; Garbossa et al., 2005; Nogueira-Campos et al., 2012; Santiago et al., 2007; Torres et al., 2006; Vlasenko et al., 2008), how the structure of such nitrergic circuits is organized across different brain processing networks has not been fully elucidated (Freire et al., 2012).

We aimed to analyze Type I neurons because they present intense Golgi-like staining of the cell body and dendrites and large somas. Type 2 neurons are smaller with lighter labeling of the cell body and, occasionally, some labeling in primary neurites (Dawson et al., 1991; Franca et al., 2000; Freire et al., 2004; Lüth et al., 1994; Sandell, 1986; Yan & Garey, 1997). These descriptions allowed a detailed morphological analysis of these classes of neurons.

As shown for excitatory pyramidal neurons, geometric characteristics of an identified neuronal subpopulation are likely to differ across functionally distinct cortical areas, reflecting local properties of vertical and horizontal processing flows (Elston, 2002; Elston et al., 2006). Since NO release may affect local neurovascular dynamics (Haselden et al., 2020) in a spatially restricted zone around the dendritic field, comparing the cortical distribution and the fine morphological arrangement of dendritic arbors of NNs across distinct cortical processing fields or compartments should contribute to a better understanding of how inhibitory NNs relate to local processing circuits.

Robust and widely used models for exploring details of cortical circuit organization are the rodent primary somatosensory cortex (S1) and primary motor cortex (M1), since each cortical region contributes with its distinct computational flow, from processing afferent sensory information to generating motor output signals (Morandell & Huber, 2017; Tandon et al., 2007). Both areas display a topographically organized and complete representation of the contralateral body (Donoghue et al., 1990; Hall & Lindholm, 1974; Tandon et al., 2007), but each of them is characterized by its specific pattern of laminar organization: S1 has six distinct layers between the pial surface and the white matter with a prominent granular Layer IV, whereas the GL is absent from M1. Notably, areas S1 and M1 share a common cytoarchitectonic border at the level of forepaw representation in rats (Donoghue & Wise, 1982; Hall & Lindholm, 1974; Petersen, 2007), providing a highly suitable location for comparing the detailed morphology of NN neurons across functionally related and neighboring

cortical fields. Since both regions of interest are present in the same histological section, such an experimental design minimizes any bias resulting from histochemical processing or intraindividual variability.

The sensorimotor hypothesis suggests that all the functions of the central nervous system are intended to convert sensory information into appropriate motor responses (Wolpaw, 2007). Therefore, it is understandable that the generation of motor commands is distributed throughout the CNS, from the cortex to the spinal cord, with no area being fully responsible for any action. However, although the motor system is highly complex, with the participation of several brain and nonbrain structures in the generation of coordinated movement and despite the difficulty in defining specific functions to specific structures in this system, M1 is recognized as a higher hierarchical region that is fundamental to coordinated voluntary movement. Several studies have been published involving electrical stimulation in M1 of anesthetized animals or recording of electrical activity in M1 of awake animals to generate movements in the animal (Ethier et al., 2006; Graziano et al., 2002) or in electronic devices (Chapin et al., 1999; Serruya et al., 2002; Wessberg et al., 2000), respectively. Capaday (2004) suggests that the motor cortex is not the decisive site of the motor command, but once the movement decision has been established, the motor cortex synthesizes the information and sends it to motor centers in the brainstem and spinal cord. In this context, the work of Gao et al. (2003) reinforces this idea by demonstrating that a lesion in the motor cortex does not totally prevent the act of moving the vibrissae in rats but completely impairs this action in terms of coordination, speed, and amplitude of contraction of the vibrissae contralateral to the injury cortical site in addition to reducing the synchrony of the vibrissae movements on both sides of the snout. Differences in signal processing between the motor and somesthetic cortices make these areas interesting for comparing the morphology of NNs. In addition, Nogueira-Campos et al. (2012) showed by a whole reconstruction of S1 that the morphology of NN changed according to the laminar or columnar cortical compartments. These researchers suggested that it could reflect the physiology of these cells. Thus, assuming that S1 and M1 contribute with their distinct computational flow, from processing afferent sensory information to generating motor output signals (Morandell & Huber, 2017; Tandon et al., 2007), we could expect an impact on the morphology of these neurons.

In the present study, we used a 3D reconstruction system (Neurolucida, see Nogueira-Campos et al., 2012) to analyze the distribution and detailed dendritic morphology of all NADPHd-labeled Type I NNs at the cortical forepaw representation and compared geometric parameters across the different laminar compartments of neighboring S1 and M1 in individual adult rats.

2 | METHODS

2.1 | Animals, perfusion, and tissue preparation

All experimental protocols were conducted following the NIH Guide for Care and Use of Laboratory Animals (www.nap.edu/catalog/

12910.html) and were approved by the Ethics Committee for Animal Use in Scientific Research (CEUA) of the Center for Health Sciences (CCS) at Federal University of Rio de Janeiro (UFRJ, protocol # IBCCF 029). Adult Wistar rats were obtained from the animal facility of the Institute of Biological Sciences (ICB, UFRJ). All efforts were made to minimize suffering and reduce the number of animals used.

Three adult male Wistar rats of the same age and approximately the same weight (5.1–5.4 g) kept in similar conditions of light exposure (Chen et al., 2013), physical exercise (Torres et al., 2006), and emotional stress (Beijamini & Guimarães, 2006) were perfused in the summer at the same time of day, between 7:00 a.m. and 8:00 a.m. (the period of maximum enzyme activity in the rat cortex), to avoid circadian oscillations of NADPHd reactivity in the neuropil, as has been reported for the visual cortex (Hilbig & Punkt, 1997). Rats were deeply anesthetized with sodium pentobarbitone (30 mg/kg) and perfused through the left ventricle using a Milan peristaltic pump (Milano Componenti, Milan, Italy) with 250 ml of 0.9% sodium chloride followed by 300–400 ml of 4% paraformaldehyde in 0.1 M, pH 7.4 sodium phosphate buffer. The same perfusion and fixation procedures were used in all animals to avoid variations described by Matsumoto et al. (1993) and Romanelli et al. (2007).

To further reduce variability, brains were systematically processed on the same day of perfusion. After removal from the skull, a block of the left hemisphere containing the entire frontal and parietal cortices was prepared and cut into serial 150-μm-thick coronal sections using a vibratome (Leica model VT 1000S). Free-floating sections were collected in 0.1 M, pH 8.0 Tris buffer, and immediately reacted for NADPHd histochemistry as follows.

2.1.1 | NADPHd histochemistry

Sections were incubated at 37°C in a solution consisting of 0.6% malic acid, 0.03% nitroblue tetrazolium, 1% dimethylsulfoxide, 0.03% manganese chloride, and 0.1% β-NADP in 0.1 M, pH 8.0 Tris buffer, following the procedure modified by Scherer-Singler et al. (1983). To increase penetration of reagents into the section thickness, 0.75% Triton X-100 was added, and sections were incubated in a shaker for 2–4 h protected from light. The histochemical reaction was periodically monitored by inspecting one or two sections under a light microscope. When most NADPHd-reactive cell bodies displayed well-labeled tertiary dendrites, the histochemical reaction was stopped with 0.1 M Tris buffer washes. Sections were promptly mounted onto poly-L-lysine-coated glass slides and left to air-dry overnight. The next day, slides were dehydrated in alcohol, washed twice in xylene for 5 min, and coverslipped using Entellan (Merck) mounting medium.

2.1.2 | Delimitation of S1, M1, and cortical compartments

The regions of interest in this study comprised the forepaw representation in areas S1 and M1 (Figure 1(a)). According to Paxinos and
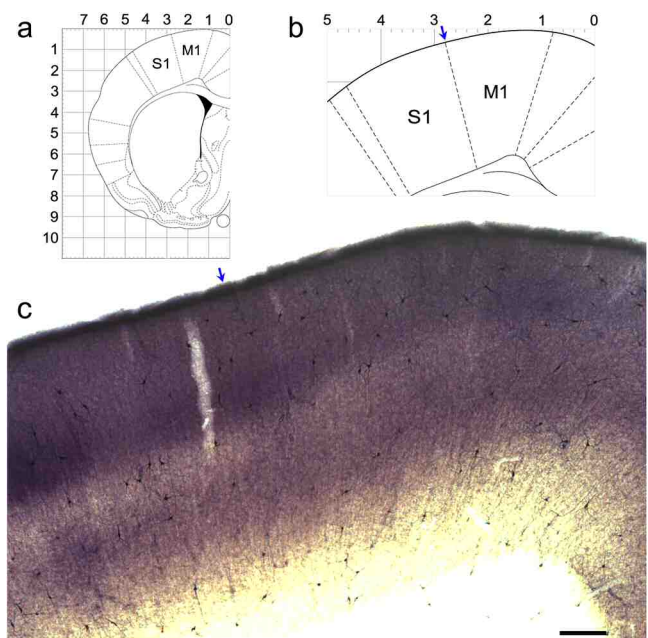

FIGURE 1 Nicotinamide adenine dinucleotide phosphate diaphorase (NADPHd) reactive neuropil and nitrergic neurons. (a) Drawing of a coronal section of the rat adult brain (Paxinos & Watson, 1997) at the level of the representation of the forepaw, enlarged in (b). (c) Photomicrograph of a coronal section at the level of the representation of the forepaw, processed for NADPHd, showing reactive neuropil and nitrergic neurons in areas S1 and M1. The representations of the forepaws in areas S1 and M1 are parallel to each other. In S1, Layer IV is more intensely labeled than Layers I–III and V-VI. Arrowheads point to the S1/M1 borders. Scale bar: 200 μm [Color figure can be viewed at wileyonlinelibrary.com]

Watson (1997), both areas share a common border along an anteroposterior extension of at least 1.0 mm, where the digits of the forepaw are represented; in this region, the medialmost portion of S1 lies side to side with the lateralmost portion of M1 (Tandon et al., 2007). According to cytoarchitectonic criteria, this border between M1 and S1 is neither sharp nor clearly delineated but rather appears as a 100-μm-wide transition zone where the laminar pattern gradually shifts from typical granular (S1) to typical agranular (M1) cortices. Therefore, the anteroposterior level of consecutive NAPHd processed sections was first defined with the aid of Paxinos's adult rat brain atlas coronal drawings using several visible anatomical landmarks, such as the size of caudate–putamen, the position of the anterior commissure, and the shape and thickness of the corpus callosum. Once coronal sections corresponding to the anteroposterior level of the forepaw were selected by gross observation, they were further examined using a ×10 objective when, based on the background staining of the neuropile, laminar boundaries could be drawn, enabling the delineation of cortical areas S1 and M1 and their common border. To avoid arbitrary misallocation of cells lying at the border, a safety region centered on the transition zone and extending 200 μm mediolaterally was adopted, and NN cell bodies lying within this sector were excluded from subsequent analyses.

Then, combinations of a cortical area with a given cortical layer-defined cortical compartments, in which we analyzed different quantitative parameters, such as neuronal density, and various morphological characteristics, such as cell body area (CBA) and dendritic length (DL; see below).

The pattern of neuropil reactivity allowed the definition of the following laminar compartments in S1, from top to bottom: (a) supragranular, or upper layers (UL, comprising cytoarchitectonically defined Layers I, II, and III), displayed intermediate background NADPHd reactivity; (b) the GL (or Layer IV) was easily distinguishable by its strong, contrasting labeling; (c) Layer V had lighter labeling; and (d) Layer VI was clearly distinguishable from the underlying white matter. The latter two layers were eventually grouped together as infragranular or lower layers (LL, comprising both Layers V and VI). Since granular Layer IV is absent from M1, this area was vertically divided into UL (I-II-III, or UL), Layers V and VI, the latter two being grouped as the LL. Thus, NNs located medially in M1 could be assigned to four laminar compartments (UL, LL, V, or VI), whereas NNs in S1, located more laterally in the coronal sections, could be assigned to five laminar compartments: UL, GL, LL (V or VI). The boundaries of each of these nine cortical compartments were drawn as quadrangular closed contours using Neurolucida software (MBFBiosciences, Inc.) under low magnification. The same registered 3D coordinate system was used to circumscribe laminar borders and plot cell bodies at low magnification, as well as to reconstruct cell bodies and dendritic arbors at much higher magnification (see below). Therefore, the Neuroexplorer companion analysis software module could compute calculations of compartment areas and volumes, as well as of neuronal densities.

2.1.3 | Stereological evaluation of NN density

The local density of NNs was evaluated in the different compartments of the forepaw representation in S1 and M1 following the procedures previously described by Nogueira-Campos et al. (2012) and using a sequence of three adjacent 150-μm-thick, NADPHd-reacted sections of the left hemisphere of three animals, thereby comprising a 450-μm-thick slab of sample cortex for each case.

Briefly, the total number of nitrergic cell body profiles (N) was counted and first divided by the flat area (A) of the respective cortical compartment. The mean density per compartment area was calculated by adding all nitrergic cell body profiles found in a given compartment in all nine sections from the three animals used in this study and then dividing this number by the sum of the compartment areas measured in each of those nine sections.

Density per volume was then estimated for each cortical compartment adopting Abercrombie's stereological correction formula (Abercrombie, 1946):

$$Nv = (N/A)/(t + d)$$

where t is the section thickness set at the vibratome (150 μm), and d is the average cell body diameter measured in each compartment. Following the procedures described by Schüz and Palm (1989), the diameter (d) was estimated from the CBA (a) using the circle formula:

$$d = 2 (a/\pi)^{0.5}$$

The average cell body diameter (d) was calculated for each cortical compartment using all reconstructed neurons located in that given compartment. Next, the value of d was corrected using the stereological estimations defined by formulas (2) and (3) of Schüz and Palm (1989), yielding values $d2$ and $d3$, respectively. Since $d2$ overestimates and $d3$ underestimates the actual value of d, the final value applied in Abercrombie's formula was the mean obtained from $d2$ and $d3$.

2.1.4 | Tridimensional reconstruction

Digital reconstruction of NN was performed using both a Zeiss ×40 neofluar plan objective (for the cell body) and a ×100 plan objective (for the dendritic tree) coupled to a Zeiss Axioplan-2 microscope equipped with a color digital camera (1600 × 1200, 3/4″ chip, 36 bit, MBF), a motorized stage (Mac5000 LUDL), and an extra z-encoder controlled by Neurolucida 8.0 software (MBFBiosciences, Inc) running on a Dell workstation.

All NNs identified in the regions under study were reconstructed, even when their dendrites spread out of the delimited areas. Some neurons whose cell bodies were located close to the cut edges of the section (as estimated by the focal plane) and/or whose dendrites disappeared abruptly at the top or bottom of the section were manifestly incomplete due to tissue sectioning. Although such incomplete neurons were partially reconstructed for quantification of neuronal density and illustration purposes, their morphometric data were excluded from the subsequent quantitative analysis. Only complete neurons, with cell bodies located in the middle of the sections and all dendrites presenting a tapering profile, were included in the quantitative analysis of morphological parameters.

2.1.5 | Acquisition of morphological parameters

The geometric properties collected during high-magnification microscopic reconstruction using the Neurolucida acquisition system may be extracted as quantitative morphological parameters using NeuroExplorer software, as previously described by Nogueira-Campos et al. (2012). These parameters were related either to the cell body or to the dendritic tree.

Cell body parameters included the following: (1) CBA, defined as the flat 2D surface occupied by the neuronal soma, and (2) form factor (FF), which varies between 0 and 1 and indicates how spherical the cell body is (values closer to 1 reflect more spherical cell body shape).

The standard morphological parameters enabling us to characterize the geometry of dendritic arborizations were as follows: (1) DL, corresponding to the sum of the lengths of all segments of the dendritic tree; (2) number of nodes, corresponding to the total number of points where two or more dendritic segments originate; (3) number of dendritic segments, defined as portions of the dendritic tree comprised between two consecutive nodes, or between a node and the cell body, or corresponding to a terminal branch; (4) dendritic field area, which measures the size of the dendritic field in a given volume or area by interpreting the branched structure as a solid object after a convex hull analysis (Wässle & Boycott, 1991); and (5) fractal dimension (FD), which gives a quantitative estimate of the complexity of dendritic arborization, describing how dendritic ramification fills the area that comprises the dendritic field.

Additionally, the dendritic orientation (6) of each neuron was defined using wedge analysis of dendritic length (dl). A Cartesian coordinate reference frame dividing eight equiangular wedges was centered at the cell body, with its principal vertical axis oriented toward the pia mater. The total length of dendritic segments enclosed in each wedge (dl_n) was measured to compute a verticality index (vi) as the sum of dl_s in the four wedges contiguous to the vertical axis, divided by the sum of dl measured in all eight wedges (total dl). vi allowed the classification of Type I neurons as horizontal- (0 < vi < 0.32), multipolar- (0.33 < vi < 0.65), or vertical-oriented (0.66 < vi < 1).

2.2 | Data analysis

All Type I NNs, labeled within a 450-μm slab, were digitally reconstructed from each of three individual animals. Cells located at the S1/M1 transition zone and incomplete cells were excluded. Morphological parameters characterizing the cell body and the dendritic tree of 380 NNs (134, 117 and 129 reconstructed from Cases 1, 2, and 3, respectively) were compared between the above defined cortical compartments of S1 and M1 forepaw representation.

A preliminary Shapiro–Wilk's W test indicated that the sample does not follow a normal distribution. Therefore, a nonparametric Kolmogorov–Smirnov two-sample test was performed, followed by computation of the maximum differences for pairs of groups and by determination of two-sided probabilities for multiple comparisons to assess statistical significance. The level of significance was set at .05 (*) and .01 (**) in all analyses. Values for morphological parameters were tabulated in a spreadsheet and transferred to Systat13 (Systat Software, Inc., Chicago, IL) for statistical analysis.

3 | RESULTS

In the following sections, we describe the pattern of NADPHd staining at the forepaw representation and then analyze the distribution and geometric parameters of cell bodies and dendritic arborizations of 380 NN before comparing their morphological properties

between neighboring cortical compartments with distinct input/output connectivity and physiological roles.

3.1 | Pattern of NADPHd-reactive neuropil staining

In rat area S1, the forepaw representation (designated S1FL by Zilles, 1985) has an anteroposterior extension of approximately 2.5 mm. However, only in its anteriormost 1.0 mm does the medial border of S1 coincide with the lateral border of area M1 (or Fr1 after Zilles, 1985). Since sensory and motor representations of the forepaw neighbor each other within the same coronal section (Brecht et al., 2004; Tandon et al., 2007), the variability inherent from NADPHd histochemical processing is reduced, allowing for direct comparison in this region of interest.

Area S1 was easily identified by the intense NADPHd reactivity of cortical Layer IV, which stood out when compared with the upper and LLs (Figure 1) and was absent from the medially neighboring area M1. Additional differences in the staining intensity of the diffuse NADPHd-reactive neuropil in area S1 enabled us to delineate its laminar borders. Typically, layer I corresponded to a thin, dark layer below the pial surface. Below are the less reactive Layers II and III. The border between Layers II and III cannot be reliably identified by means of NADPHd histochemistry alone. Below the strongly reactive Layer IV lies the pale, poorly reactive Layer V. Layer VI displays an intermediate intensity of staining (Figure 1(c)).

In a typical coronal section, as one progresses from S1 toward the midline (Figure 1), the rather abrupt termination of Layer IV indicates the transition from S1 to area M1, which is characterized by a more homogeneous pattern of neuropil staining, where UL (I–III) and LL (V-VI) display staining patterns similar to the staining patterns observed in S1. In M1, Layers II and III display intense and almost uniform background staining, whereas subjacent Layer V is the palest cortical layer, and Layer VI displays an intermediate level of NADPHd reactivity, as in S1. However, Layers V and VI both appear slightly more intensely labeled in M1 than their respective counterparts in S1 (Figure 1(c)).

3.2 | Cortical distribution and density of NNs

To quantify the spatial distribution of NNs in the different cortical compartments of S1 and M1, neuronal density was calculated for each case after adding up the number of cell bodies and the area size of delineated cortical compartments in S1 and M1 from all selected sections (Table 1). Since simple cell counting may result in biased estimations of the number of cellular profiles (Gundersen et al., 1988), appropriate stereological corrections were applied (see Section 2). Once all measured compartment areas were added from the set of selected sections, the size of the forepaw representation averaged 7.47 mm^2 for S1 and 7.26 mm^2 for M1. LLs accounted for 60% of the cortical thickness in both S1 and M1, and correspondingly, these layers contained 50–60% of all NNs found

TABLE 1 Distribution of NNs cell bodies in the different cortical compartments

Cortical compartments[a]	Number of cells		Compartment area (mm^2)		Cell body diameter (SEM) in μm		Neuronal density (cells/mm^3)[b]	
	S1	M1	S1	M1	S1	M1	S1	M1
Total area	206	174	7.47	7.26	12.95 (0.1)	13.15 (0.1)	130	119
UL (I–III layers)	75	83	1.77	2.93	13.46 (0.2)	13.09 (0.2)	156	149
GL (IV layer)	21	—	1.03	—	13.11 (0.3)	—	125	—
LL (V-VI layers)	110	91	4.68	4.33	12.58 (0.8)	13.22 (0.2)	121	99
Layer V	44	49	2.5	2.6	13.04 (0.3)	13.11 (0.3)	84	99
Layer VI	66	42	2.17	1.73	12.28 (0.2)	13.35 (0.3)	165	100

[a]Cortical compartments: GL, granular layer; LL, lower layers; SEM, standard error of the mean; UL, upper layers.
[b]Corresponding values were calculated after stereological corrections described in section "Stereological Evaluation of Cell Density" (see Section 2).

in the region of interest. Layer V displayed the lowest density values in both S1 (84 neurons/mm^3) and M1 (99 neurons/mm^3). However, the highest NN density values were observed in Layer VI for S1 (165 neurons/mm^3) and in the ULs for M1 (149 neurons/mm^3). Overall, the average NN density was slightly higher in S1 (130 neurons/mm^3) than in M1 (119 neurons/mm^3).

3.3 | Morphology of NNs in the forepaw representation

We reconstructed all NADPHd neurons within the selected parts of areas S1 and M1 in three sequential sections for three rats (two shown in Figure 2(a,b)). Cells located at the limits between two contiguous compartments were assigned to the compartment including more than half of the cell body. All ramifications of a given NN were assigned to the compartment containing its cell body, irrespective of whether parts of the dendritic tree were located in a neighboring compartment. Neurons were grouped into nine possible compartments, four within M1: (a) UL (Layers I–III); (b) Layer V; (c) Layer VI; (d) the latter being eventually grouped with Layer V as LL (Layer V-VI); and five in S1, characterized by its prominent, densely stained GL (Layer IV), absent from M1. Figure 2 shows all NNs in consecutive sections, while Figures 3, 4, and 7 illustrate representative individual neurons reconstructed from those nine compartments.

Figure 3 shows micrographs and flattened 3D reconstructions of two Type I neurons, one from S1 Layer IV (a, c, e) and another from M1 ULs (b, d, f). Both cells display a similar number of primary dendrites, and their arborization extends over a similar area, where the cell body occupies a central position.

Figure 4 illustrates four other examples of NNs whose cell bodies were located in the UL of area S1 (a), UL of M1 (b), LL of S1 (c), or LL of M1 (d). These neurons display dendritic fields of different sizes and different orientations relative to the pial surface. Their cell bodies also display different sizes and are asymmetrically located within the volume enclosing the entire dendritic arborization. Below, we analyze and compare the quantitative parameters characterizing the morphology of NNs at the forepaw representation.

3.4 | Quantitative analysis of NN morphological parameters

Morphological parameters describing the cell body (CBA and FF) and dendritic branching (DL, dendritic field, number of nodes and segments, FD, and vi) of the 380 reconstructed NNs were compared across both cortical areas and their nine laminar compartments. Comparisons are expressed as medians, first and third quartiles, maxima and minima (box plots on the left in Figure 5) and individual values (scatter plots on the right in Figure 5).

Figure 5 shows that NADPHd-positive neurons in S1 displayed a higher vi than the NADPHd-positive neurons in M1 ($p < .05$). There was no significant difference between S1 and M1 samples for CBA, DL, dendritic field, number of nodes, or FD.

Figure 6 shows a quantitative evaluation of the significant differences in the morphological parameters observed between cortical compartments of S1 and M1. Figure 6(a) shows the significant differences in CBA for S1 (blue) and M1 (red) cortical compartments. In S1, NADPHd neurons in the UL display larger somas than the NADPHd neurons reconstructed in the LL. This difference is particularly evident for S1 Layer VI, which displays the lowest mean CBA of all compartments sampled in S1 or M1. LL neurons of M1 have larger soma than LL neurons of S1.

Figure 6(b) shows the significant differences in the cell body FF across cortical compartments. Neurons from S1 LL are more spherical than the neurons from M1 LL, especially from M1 Layer VI, which contains the largest proportion of cells with low FFs.

Regarding dendritic field area (Figure 6(c)), neurons in the UL of S1 displayed a larger total DL than Layer VI neurons from the same cortical area. Neurons of the GL display significantly larger DLs than the neurons from the upper or LLs of S1. In turn, the dendritic arbors of LL neurons of M1 cover larger field areas than the dendritic arbors of S1 LL. Figure 6(d) shows no significant differences in the DL of neurons labeled in the different cortical compartments of S1 or M1 ($p < .05$).

Figure 6(e,f) presents the statistical distributions for the number of nodes and segments, respectively ($p < .05$). Since both parameters are intrinsically related, they actually follow the same pattern. Within S1, UL neurons have more nodes and segments than the neurons

FIGURE 2 3D reconstruction of all Type I nitrergic neurons (NNs) labeled in the forepaw representation in areas S1 and M1 of two adult rats, shown in different cytoarchitectonic compartments. All NNs reconstructed from three selected contiguous sections of case one (a) and case two (b) are shown with random coloring. NNs are more densely packed in the upper layers (I–III) and more sparsely distributed in Layer V. the distribution of labeled somas differs between S1 and M1. In M1, most NNs are in the upper layers. In S1, labeled cells are distributed both in upper layers and in Layer VI, while only a few NNs are in Layer V. dorsal is to the top, medial to the right. Scale bar: 100 μm [Color figure can be viewed at wileyonlinelibrary.com]
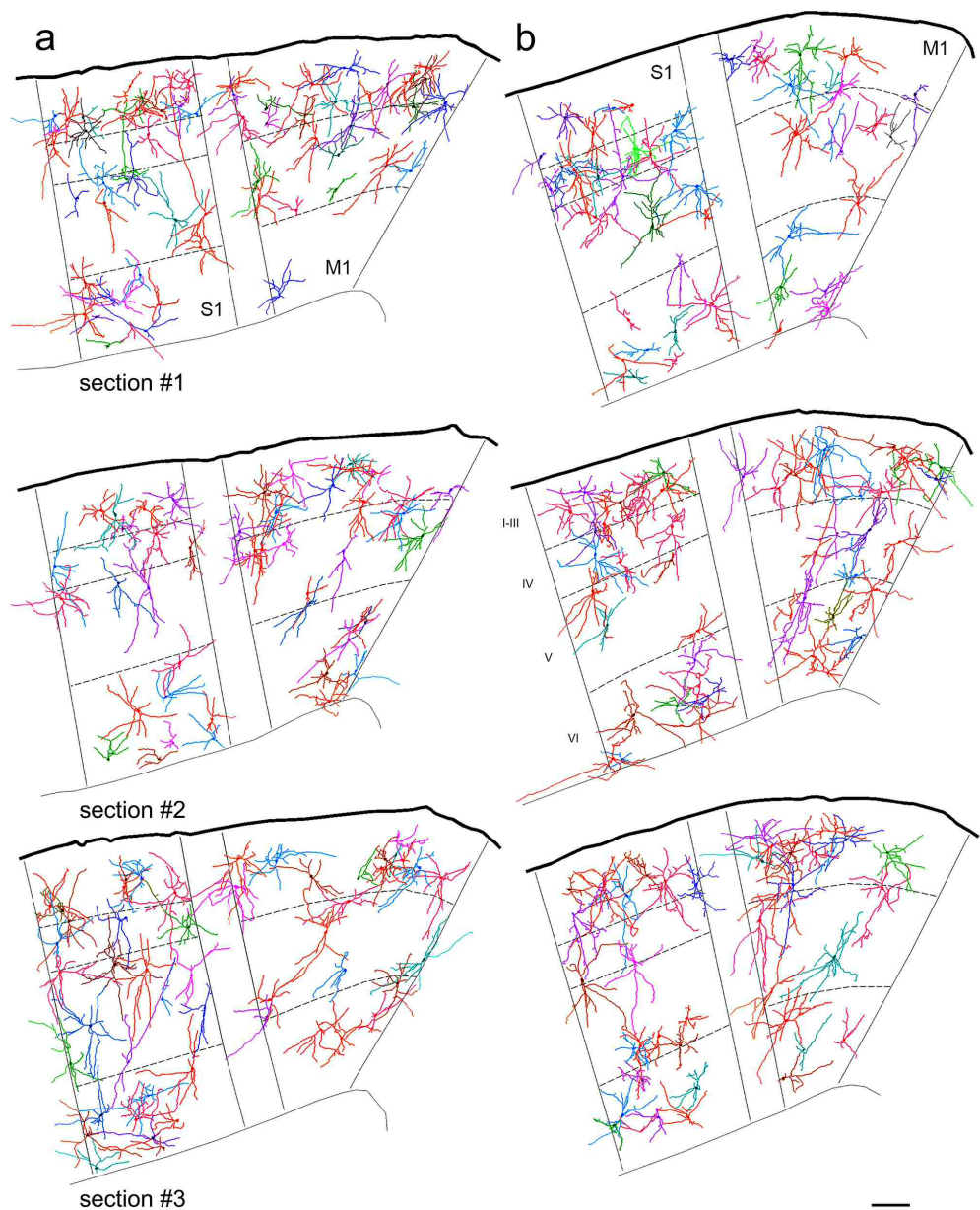
located in LL. The dendritic trees of GL neurons display more nodes and segments than NN neurons from any other compartment of S1 or M1. When both areas are compared, UL neurons display fewer nodes or segments in S1 than in M1.

Figure 6(g) shows the differences in the FD of NNs across cortical compartments. As might be expected from their larger values for nodes, segments, DL, and field area, NN in S1 Layer IV displays a wider FD than the NNs in upper or LLs from S1 or M1.

Figure 6(h) shows the differences in the vi. The vi was computed after a wedge analysis of the distribution of dendritic segments, yielding values closer to 1 for trees oriented mostly parallel to the axis of radial cortical columns (vertical neurons), while values closer to 0 indicated that dendritic branches were primarily oriented parallel to the cortical layers (horizontal neurons, see Section 2). Neurons with intermediate vi were classified as multipolar since they did not present any preferred segment orientation. In S1, neurons from Layer V display higher verticality indices than the neurons from UL or Layer VI, while Layer VI neurons display lower vi than those of GL. In M1, UL neurons have smaller verticality indices than LL NNs. When comparing both areas, GL neurons in S1 showed a higher vi than UL neurons in M1. Furthermore, dendritic arbors of Layer V neurons in S1 appear more vertically oriented than neurons of any compartment of M1.

Figure 6(i) gives confidence levels of all statistical comparisons for each morphological parameter across compartments. No significant difference was observed in the DL between any two compartments. However, the comparison between S1 and M1 reveals differences for lower-layer neurons in CBA, number of nodes (#N), number of segments (#S), and FD. The most significant differences were noted within area S1, between Layer IV and the ULs, or between Layers IV and VI. This trend in the differences in the vi contrasted with the distribution of other geometric parameters (see Figure 6(i)). Overall, differences in morphological parameters were frequent in the
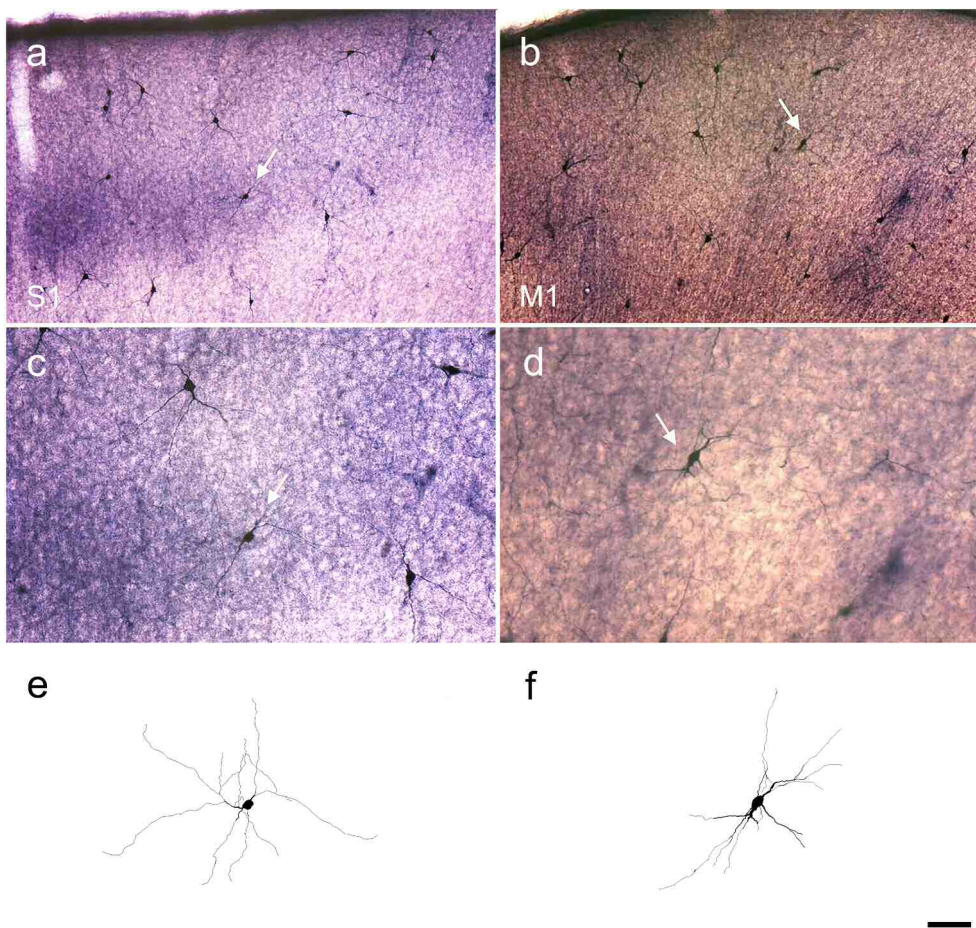
FIGURE 3 Photomicrographs and 3D reconstructions of two nicotinamide adenine dinucleotide phosphate diaphorase (NADPHd)-labeled neurons in areas S1 and M1. Examples of nitrergic neurons (NNs) labeled after NADPHd histochemistry in Layer IV of area S1 (left: a, c, e) and in the upper layers of area M1 (right: b, d, f). Top, low magnification photomicrograph allowing us to appreciate background reactivity of the neuropil. Middle, closer view emphasizing a selected neuron at the same magnification as its reconstruction shown below. Bottom, complete 3D reconstruction of the neuron highlighted in the above microphotograph. White arrows point to the selected neuron in each example. The scale bar at the lower right is 100 μm for panels a and b and 50 μm for Panels (c–f) [Color figure can be viewed at wileyonlinelibrary.com]

comparisons between different laminar compartments of S1 and rare between M1 compartments. The results suggest that differences in the morphological characteristics between S1 and M1 NNs are most evident in LLs V and VI.

Finally, Table 2 describes the areal and laminar distribution of all NNs according to their main dendritic orientation, as defined from the ranges of vi values (see Figure 6). Most NNs in our sample were multipolar (63%, 0.33 < vi < 0.65) or vertical (28%, vi > 0.66), while a minority were horizontal (9%, vi < 0.32). In S1, 58% of the NNs were multipolar, 36% vertical, and only 6% horizontal. Multipolar NNs were more common in the UL (n = 23), vertically oriented neurons were prominent in Layer V (n = 15), and most horizontally oriented neurons were observed in Layer VI (n = 4). In M1, the proportion of multipolar NNs was even higher (68%), whereas vertical and horizontal NNs represented 20 and 12%, respectively. In M1, multipolar NNs were more frequent in the ULs (n = 41), followed by Layer VI (n = 15), while vertical NNs were more common in Layer V (n = 8) and horizontal neurons in the UL (n = 9).

4 | DISCUSSION

We described and compared the distribution and morphological arrangement of NADPHd-labeled Type I NNs within the forepaw representation of neighboring cortical areas S1 and M1 of adult Wistar rats. These cells constitute a subpopulation of inhibitory GABAergic neurons capable of releasing NO, a small gaseous molecule involved in several fundamental physiological and pathological roles in peripheral and central nervous systems (Bredt & Snyder, 1992; Dawson et al., 1994). How the neurochemical, electrophysiological and morphological properties of inhibitory, NO-releasing neurons may relate to local vascular and/or neuronal networks remains unclear (Cauli & Hamel, 2010). However, since the diffusion of NO is fast, transient and spatially restricted, the geometric features of NNs are likely to reflect their contribution to the local regulation of cerebral blood flow dynamics, which also depends on the local features of the cortical circuit (including neural excitatory and glial elements, as well as on their modulation by diffuse subcortical inputs). Therefore, we explored and compared the morphological properties of NN between two strongly interconnected areas that are widely used for modeling cortical processing: the primary sensory and motor cortices of the rat.

Both areas S1 and M1 are topologically organized to provide a map of the contralateral body parts and, at the level of the forepaw representation, lie close to each other, sharing a common transition zone. However, S1 and M1 have distinct input/output connectivity, laminar patterns, and horizontal and vertical circuit organizations and perform distinct operations during sensorimotor processing
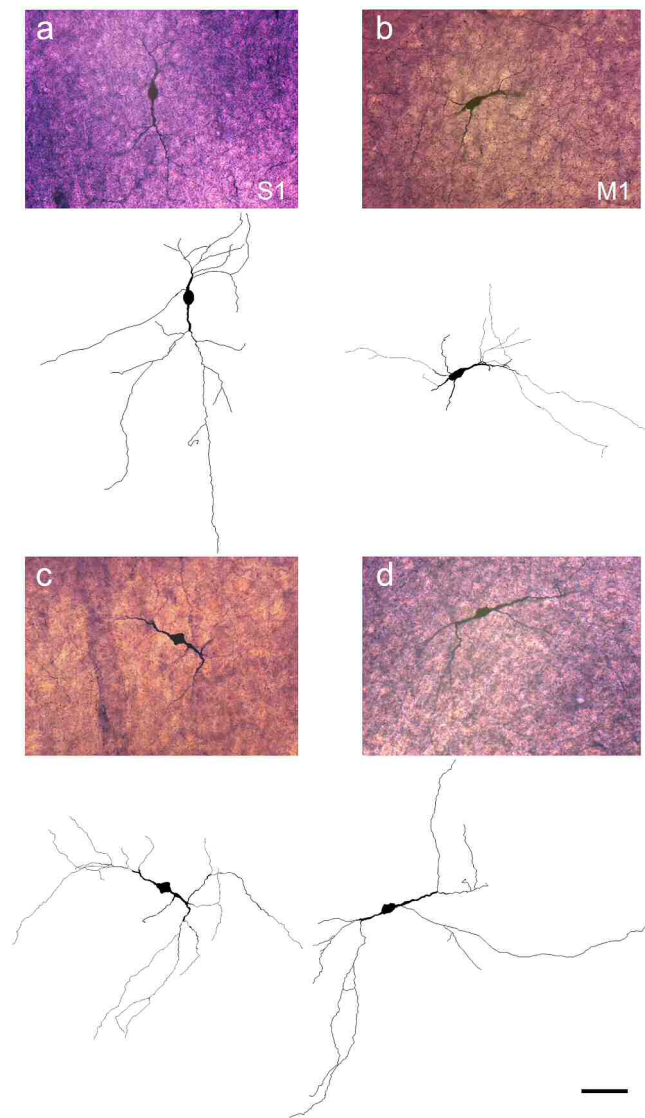
FIGURE 4 Photomicrographs and 3D reconstructions of four nicotinamide adenine dinucleotide phosphate diaphorase (NADPHd)-labeled neurons in areas S1 and M1. Photomicrographs and reconstructions of four examples of NADPHd-labeled neurons from the forepaw representation located in: (a) S1 upper layers, (b) M1 upper layers, (c) S1 lower layers, and (d) M1 lower layers. Scale bar: 50 μm [Color figure can be viewed at wileyonlinelibrary.com]

FIGURE 5 Comparison of morphological parameters for nitrergic neurons in S1 (red) and M1 (blue). Median (heavy line), first and third quartiles (box), maximum and minimum (vertical lines), and individual values (circles) of six parameters used to describe and quantify the soma and dendritic arbors of all nitrergic neurons reconstructed in our sample. For the verticality index graph (bottom, right), the yellow band corresponds to horizontal neurons (vi = 0–0.32), the white band (vi = 0.33–0.65) to multipolar neurons, and the green band to vertical-oriented cells (vi = 0.66–1). Asterisk (*) indicates a significant difference of $p < .05$ [Color figure can be viewed at wileyonlinelibrary.com]

(Donoghue et al., 1990; Donoghue & Wise, 1982; Lübke & Feldmeyer, 2007; Tandon et al., 2007; Wester & Contreras, 2012). In the present study, we explored these shared and distinct characteristics to investigate whether the cortical distribution and morphology of NNs may relate to the layout of local processing modules.

4.1 | Distribution of NNs in areas S1 and M1

We found several differences in the distribution and density of NN across the forepaw representation in S1 and M1. Globally, the density
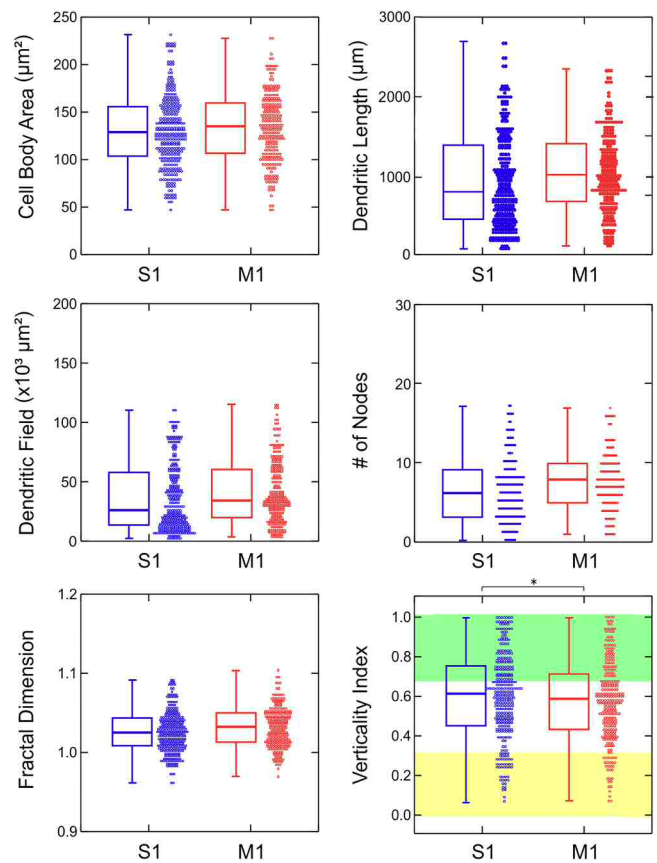
of NNs was higher in S1 than in M1. Similar results were observed for the distribution of NN in other parts of the body representation in S1 and M1 (Huh et al., 1998) and, more recently, in the extensively studied region of whisker representation (Afarinesh & Behzadi, 2018).

After dividing the selected region of interest into several cytoarchitectonic compartments, we observed that Layer VI of the S1 forepaw representation contained the highest density of NNs (165 cells/mm^3) in keeping with a previous study focused on the whisker pad representation in S1 (Afarinesh & Behzadi, 2018). As the cortical thickness was divided into UL (Layers I–III), GL (Layer IV), and LLs (including Layers V and VI), higher NN density values were observed in UL, consistent with Nogueira-Campos et al. (2012), who analyzed the distribution of NN throughout the entire S1 cortex, including its representations of the snout, whiskers, trunk, hind-, and forelimbs. Other studies of the distribution of NN in S1 (Franca et al., 2000; Freire et al., 2004) have been performed mostly on serial, tangential
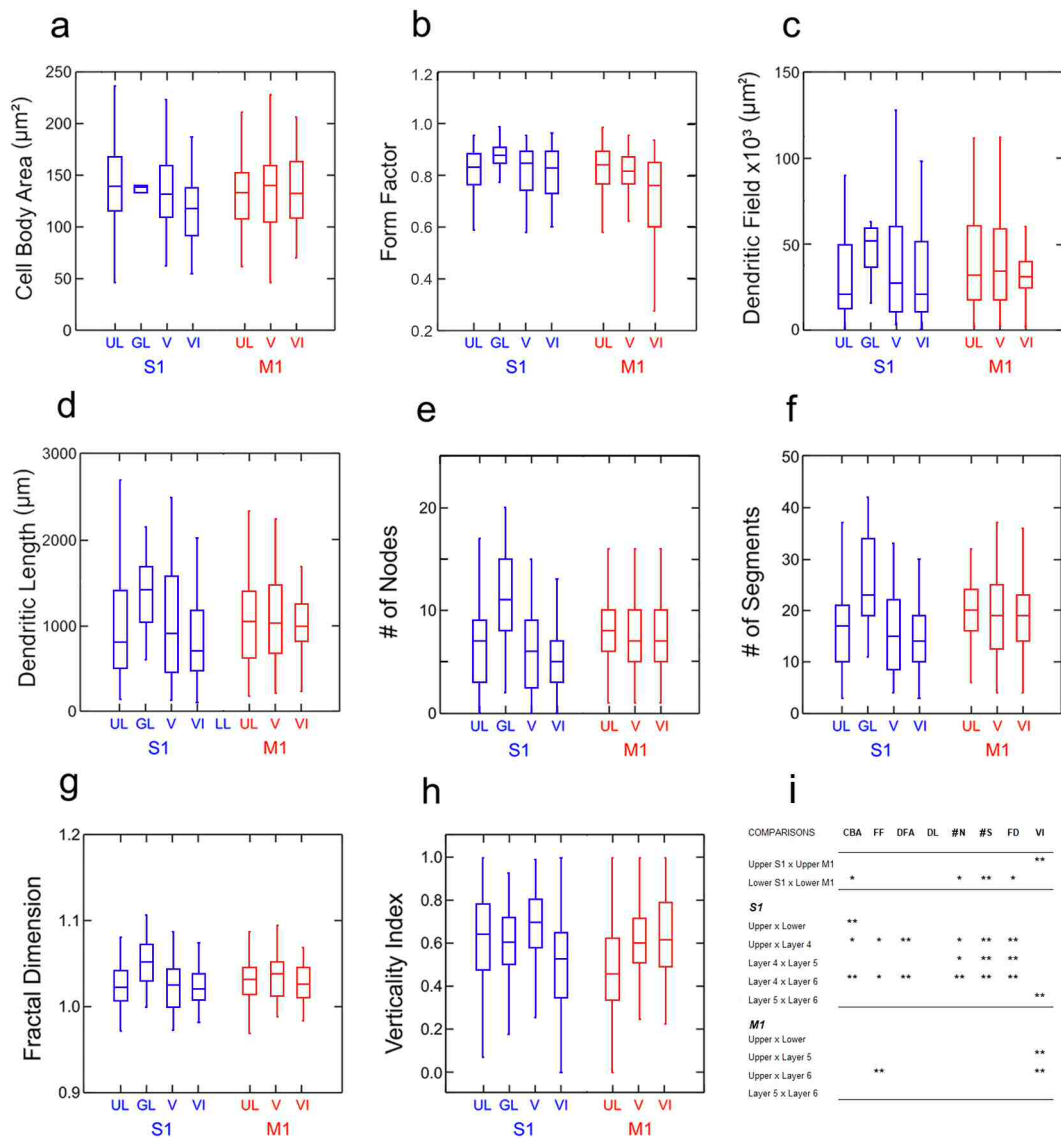
FIGURE 6 Comparison of morphological parameters for nitrergic neurons reconstructed from different cortical compartments of areas S1 and M1. Median (heavy line), first and third quartile (box), maximum and minimum (vertical lines) values for the following variables computed for the 380 reconstructed nitrergic neurons: (a) cell body area (CBA); (b) form factor (FF); (c) dendritic field area (DFA); (d) dendritic length (DL); (e) number of nodes (#N); (f) number of segments (#S); (g) fractal dimension (FD); and (h) verticality index (VI). Data were grouped according to area (blue, S1; red, M1) and their laminar compartments (UL, upper layer; GL, granular layer; V, Layer V; and VI, Layer VI). (i) Table indicating significance values for all comparisons across areas and compartments. (*) $p < .05$ and (**) $p < .01$ [Color figure can be viewed at wileyonlinelibrary.com]

sections parallel to Layer IV of the posterior medial barrel subfield (where individual whiskers are represented discretely in sharply defined barrels). These estimates of the laminar distribution of NN indicated higher densities in the supragranular layers and in Layer VI, compatible with our present results.

Within the forepaw representation of area M1, the highest NN density was found in UL, followed by Layer VI. Other studies in M1 reported the most numerous NNs in Layer V (in the whisker representation, Afarinesh & Behzadi, 2018) or in Layer VI (Vlasenko et al., 2008), although the last study does not state explicitly which parts of M1 were actually selected in the counted sections. Such discrepancies may indeed result from the sampling of different parts of M1 representations across these studies. Further work and approaches will be necessary to better correlate the distribution of NNs within cortical area M1 modules and layers and, therefore, to better understand how the nitrergic network contributes to cortical physiology and dynamics.

4.2 | Morphological variability of NNs within S1 and M1

4.2.1 | Local diversity of morphotypes

Based on the median values of all morphological parameters from each cortical compartment, "typical" representative neurons could be

TABLE 2 Distribution of NNs according to their dendritic orientation

	Vertical			Multipolar			Horizontal		
	S1	M1	Total	S1	M1	Total	S1	M1	Total
Total area	39 (18%)[a]	20 (10%)[a]	59 (28%)[a]	62 (30%)[a]	70 (33%)[a]	132 (63%)[a]	6 (3%)[a]	12(6%)[a]	18 (9%)[a]
UL (I–III layers)	9 (4%)[a]	8 (9%)[a]	17 (19%)[a]	23 (11%)[a]	41 (20%)[a]	64 (31%)[a]	1 (1%)[a]	9 (4%)[a]	10 (5%)[a]
GL (IV layer)	9 (4%)[a]	—	9 (4%)[a]	9 (4%)[a]	—	9 (4%)[a]	—	—	—
LL (V-VI layers)	21 (10%)[a]	12 (12%)[a]	33 (33%)[a]	30 (15%)[a]	29 (13%)[a]	59 (28%)[a]	5 (2%)[a]	3 (2%)[a]	8 (4%)[a]
Layer V	15 (7%)[a]	8 (16%)[a]	23 (45%)[a]	11 (6%)[a]	14 (6%)[a]	25 (12%)[a]	1 (1%)[a]	2 (1%)[a]	3 (1%)[a]
Layer VI	6 (3%)[a]	4 (8%)[a]	10 (20%)[a]	19 (9%)[a]	15 (7%)[a]	34 (16%)[a]	4 (1%)[a]	1 (1%)[a]	5 (3%)[a]

[a]Number of NNs per compartment and rounded percentage of the total number of NN reconstructed in the sample = 209 NN (107 in S1 and 102 in M1); total: sum of NN in S1 and M1.

Abbreviations: GL, granular layer; LL, lower layer; NNs, nitrergic neurons, UL, upper layer.

selected for each layer of S1 and M1. Figure 7 illustrates a set of such representative neurons, which display the CBA, FF, DL, number of nodes, number of segments, FD, and vi values close to the median computed for each compartment. However, our data confirm that the heterogeneity of NN morphotypes is observed even within a restricted laminar and modular piece of cortex. As shown in the reconstructions in Figure 1, dendritic arbors of neighboring NNs may span restricted or extensive cortical volumes and assume any orientation. Defining the range of these structural parameters is useful to elaborate cortical models that may integrate the biologically observed local diversity of inhibitory nitrergic morphotypes in addition to their known patterns of spontaneous and evoked firing properties and to the range of possible neurochemical profiles. In the present study, we applied only NADPHd histochemistry to optimize staining contrast and allow for detailed reconstruction of fine processes throughout consecutive 150-μm-thick sections. New approaches for spine visualization and reconstruction may contribute to classifying subtypes of NN (Pchitskaya & Bezprozvanny Ilya, 2020), although such categorization remains an open issue. Further studies combining additional markers are required to investigate how the diverse phenotypic characteristics of NNs may contribute to the modulation of cortical dynamics (see Cauli & Hamel, 2010; Kubota et al., 2011).

4.2.2 | Cell body size and shape

The size and shape of NN cell somas were assessed by computing CBA (CBA) and FF (yielding values ranging from 0 to 1, corresponding to more elongated or more spherical shape, respectively). No significant difference in these parameters was noted between areas S1 and M1 when these areas were considered globally. However, differences were evident across cortical compartments. The somas of NN in the LLs of M1 were significantly larger ($p < .05$) and more elongated than the somas of NN in S1 LL. Afarinesh and Behzadi (2018) observed opposite results and reported a smaller mean soma diameter in M1 than in S1. However, their region of interest was the whisker representation, while we

focused on the forepaw representation. In any case, our results reveal differences in the laminar distribution of soma size and shape between S1 and M1, which are discussed below.

Within S1, GL NNs displayed larger somas than the other layers, in agreement with the findings of Nogueira-Campos et al. (2012) in S1 and compatible with the abundant literature confirming the intense NADPHd histochemical reactivity of Layer IV in primary sensory areas (Wallace, 1987; Wong-Riley & Welt, 1980), which also appears strongly reactive for metabolic enzymes such as succinate dehydrogenase or cytochrome oxidase (Aoki et al., 1993; Wong-Riley et al., 1998), reinforcing the hypothesis that heavy NOS expression might be related to sustained afferent neural activity (Garthwaite & Boulton, 1995). Importantly, however, pharmacological experiments suggested that neuronal NO release does not mediate the stimulus-induced metabolic response but rather plays a permissive role by increasing local blood flow (Lindauer et al., 1999) and thus modulates the level and, possibly, the saliency of evoked signals. The relative contribution from the soma and from diffuse reactive neuropiles to NO release also remains to be clarified. Whereas the largest NN cells were found in GL in S1, NNs located in Layer VI displayed significantly ($p < .01$) smaller somas than NNs located in other layers (Figures 6 and 7).

In contrast, within the M1 forepaw region, Layer VI NN was significantly ($p < .01$) more elongated than in other layers (Figures 5–7). Large and elongated NN somas may be associated with specific modulatory requirements for layers involved in the generation of motor output signals. There is no consensus regarding the spatial–temporal dynamics of basal or evoked NO release by cortical neurons (Cauli & Hamel, 2010) or whether and how soma shape actually influences the release of gaseous NO or of coexpressed classical neuromodulators.

4.2.3 | Dendritic field complexity, size, and orientation

In the present study, we did not find any significant differences in the total DL of NNs throughout the forepaw representation. However,
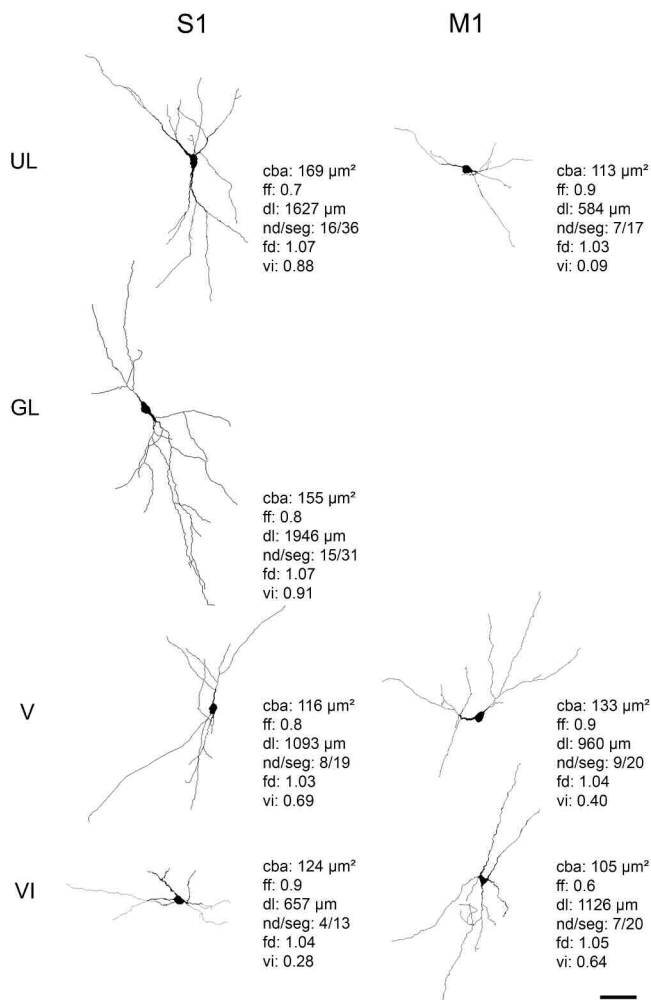
S1   M1

UL

cba: 169 µm²
ff: 0.7
dl: 1627 µm
nd/seg: 16/36
fd: 1.07
vi: 0.88

cba: 113 µm²
ff: 0.9
dl: 584 µm
nd/seg: 7/17
fd: 1.03
vi: 0.09

GL

cba: 155 µm²
ff: 0.8
dl: 1946 µm
nd/seg: 15/31
fd: 1.07
vi: 0.91

V

cba: 116 µm²
ff: 0.8
dl: 1093 µm
nd/seg: 8/19
fd: 1.03
vi: 0.69

cba: 133 µm²
ff: 0.9
dl: 960 µm
nd/seg: 9/20
fd: 1.04
vi: 0.40

VI

cba: 124 µm²
ff: 0.9
dl: 657 µm
nd/seg: 4/13
fd: 1.04
vi: 0.28

cba: 105 µm²
ff: 0.6
dl: 1126 µm
nd/seg: 7/20
fd: 1.05
vi: 0.64

FIGURE 7 Selected representative nitrergic neurons (NNs) 3D-reconstructed from each cytoarchitectonic compartment in areas S1 and M1. Representative NNs were selected on the basis of median values observed for each cortical compartment (see text). All NNs are oriented as if the pia mater was parallel to the top of the figure. Left column, area S1; right column, area M1. From top to bottom: UL, upper layers (I-II-III); GL, granular layer IV; V and VI, LLs V and VI. The NN in S1 display more vertically-oriented dendritic trees, whereas NN in M1 tend to be multipolar or horizontally oriented. Values of four relevant morphological parameters for each representative neuron are indicated: cba, cell body area; ff, form factor; dl, total dendritic length; nd, nodes; seg, segments; fd, fractal dimension; vi, verticality index. Scale bar: 50 µm

significant intraareal and interareal differences in the complexity of dendritic arbors were detected, as expressed by variations in the number of nodes or segments, FD and dendritic field size.

Within S1, GL NN had a higher FD and more nodes and segments than NNs from other layers. UL NNs also had more nodes and segments and occupied a larger dendritic field area than NNs in LL, especially than NNs in Layer VI. Within M1, no difference in the dendritic field area was found across laminar compartments. When comparing both areas, M1 UL NNs had fewer nodes and segments and smaller FD than S1 NNs located in UL or GL (Figures 6 and 7). This finding is

consistent with Afarinesh and Behzadi (2018), who reported fewer third-order dendritic branches, nodes and segments of NNs in M1 than in S1.

The analysis of NN dendritic field orientation in the forepaw representation showed that most NNs are multipolar or vertically oriented. Globally, S1 NN displays higher vertical indices than NNs in M1. Such bias in favor of vertically oriented dendritic fields in S1 was especially significant in UL ($p < .01$), although S1 Layer V NN also displayed a higher vi than M1 NN in any laminar compartment (Figures 6 and 7).

Throughout S1, the majority (58%) of NNs were multipolar, over a third (36%) were vertically oriented, and only a minority (6%) were horizontal (Table 2). The proportion we found for the primary somatosensory forelimb representation differs from the values reported by Nogueira-Campos et al. (2012) for the entire S1 area (50% vertical, 24–29% multipolar, and 7–26% horizontal NNs). Since both studies used similar conditions for animal breeding, identical procedures for tissue preparation and processing, and applied the same criteria for data analysis, it is likely that the observed discrepancy actually reflects differences in the sampled areas of S1. We concluded that dendritic fields of NN in Layer V are more vertically oriented than those in Layer VI or in the UL of S1 (Figure 6). We also noted that the S1 GL NNs had higher verticality indices than NNs in the underlying layers (Layer VI), although this tendency did not hold when both LL (V and VI) were grouped together. Nogueira-Campos et al. (2012) observed significantly lower verticality indices in UL than in other layers of S1 but did not distinguish Layer V from Layer VI.

In M1, UL neurons displayed a lower vi than in other layers (Figure 6). To the best of our knowledge, no extensive examination of NN in M1 is available to date, thereby precluding a comparison of our data for M1 compartments.

Since differences in the geometric characteristics of cell bodies and dendritic fields of NNs vary across cortical layers within the forepaw representation of S1 and M1, we suggest that individual cells with larger somas, larger numbers of nodes and segments, higher FDs, and wider dendritic fields have larger volumes and may contribute to the higher concentration of NO-synthesizing enzymes across layers. A less vertically oriented NN in the UL of S1 may contribute to sustaining the metabolic demands necessary for horizontal integration through tangential connections. At the same time, the NN in GL and Layer V may maintain vertical processing throughout cortical thickness (Schubert et al., 2007).

5 | CONCLUSIONS

GABAergic inhibitory cortical neurons represent a phenotypically diverse population. Such diversity is expressed by the variable electrophysiological, neurochemical, and morphological characteristics observed across species and brain regions. NO-releasing neurites may influence neurometabolic dynamics in different manners according to

their relationships with the local microvascular network and with glial elements. In addition, their modulatory influence is also likely related to their integration within local neuronal networks.

We explored such relationships in the rat cortex, specifically in the forepaw representation of S1 and M1. When both areas were compared globally, the diversity of NN morphotypes seems preserved across both cortical fields, since they share a similar distribution of soma and dendritic field characteristics, although NNs are slightly more numerous in S1 than in M1. However, when cortical areas were divided into laminar compartments, morphological differences appeared between S1 and M1, suggesting that different NN morphotypes may influence neuronal NO release in a distinct way across the cytoarchitectonic compartments of primary areas specialized in processing sensory inputs and generating motor outputs.

However, cortical GABAergic neurons can be parceled into a number of subgroups based on variations in morphology, birthplace, mature locations, colocalized peptides, and electrophysiological parameters. Despite such diversity, conventional models of cortical function include GABAergic neurons as participators only in local connectivity that play an inhibitory role. However, cortical GABAergic categories include a subset of phylogenetically conserved neurons that project axons across long distances, known as cortical GABAergic projection neurons. Thus, it is possible that GABAergic projection neurons might be a subset of the little-studied cells that persist in the adult brain from the developmental subplate, and some NADPH-d neurons could be long-range NOS neurons (Clancy et al., 2010).

CONFLICT OF INTEREST

We declare that there is no conflict of interest, either financial, personal or other relationships with other people or organizations within 4 years of beginning the submitted work that could inappropriately influence the results or interpretation of the data in the manuscript.

AUTHOR CONTRIBUTIONS

All authors had full access to all the data in the study and take responsibility for the integrity of the data and the accuracy of the data analysis. **Marco Rocha Curado**, **Bárbara de Paula Pires Franco Guimaraes**, **João Guedes da Franca**, and **Jean Christophe Houzel**: Study concept and design. **Bárbara de Paula Pires Franco Guimaraes**, **Anaelli Aparecida Nogueira-Campos**, and **Marco Rocha Curado**: Data acquisition. **Ricardo Gattass**, **Bárbara de Paula Pires Franco Guimaraes**, and **João Guedes da Franca**: Analysis and interpretation of data. **Ricardo Gattass** and **Bárbara de Paula Pires Franco Guimaraes**: Drafting of the manuscript. **Bárbara de Paula Pires Franco Guimaraes**, **Ricardo Gattass**, and **Anaelli Aparecida Nogueira-Campos**: Critical revision of the manuscript for important intellectual content. **Bárbara de Paula Pires Franco Guimaraes** and **Ricardo Gattass**: Statistical analysis. **João Guedes da Franca**, **Ricardo Gattass**, and **Jean Christophe Houzel**: Funding.

PEER REVIEW

The peer review history for this article is available at https://publons.com/publon/10.1002/cne.25192.

DATA AVAILABILITY STATEMENT

Data have not been shared. Our web repository is under construction. Data are available upon request to the first author.

ORCID

Ricardo Gattass https://orcid.org/0000-0002-0321-1490

REFERENCES

Abercrombie, M. (1946). Estimation of nuclear population from microtome sections. *The Anatomical Record*, *94*(2), 239–247. https://doi.org/10.1002/ar.1090940210

Afarinesh, M. R., & Behzadi, G. (2018). The effects of de-whiskering and congenital hypothyroidism on the development of nitrergic neurons in rat primary somatosensory and motor cortices. *Cell Journal*, *20*(2), 157–167. https://doi.org/10.22074/cellj.2018.5112

Aoki, C., Fenstemaker, S., Lubin, M., & Go, C. G. (1993). Nitric oxide synthase in the visual cortex of monocular monkeys as revealed by light and electron microscopic immunocytochemistry. *Brain Research*, *620*(1), 97–113. https://doi.org/10.1016/0006-8993(93)90275-R

Beijamini, V., & Guimarães, F. S. (2006). Activation of neurons containing the enzyme nitric oxide synthase following exposure to an elevated plus maze. *Brain Research Bulletin*, *69*(4), 347–355. https://doi.org/10.1016/j.brainresbull.2006.02.006

Brecht, M., Krauss, A., Muhammad, S., Sinai-Esfahani, L., Bellanca, S., & Margrie, T. W. (2004). Organization of rat vibrissa motor cortex and adjacent areas according to cytoarchitectonics, microstimulation, and intracellular stimulation of identified cells. *Journal of Comparative Neurology*, *479*, 360–370. https://doi.org/10.1002/cne.20306

Bredt, D. S., & Snyder, S. H. (1992). Nitric oxide, a novel neuronal messenger. *Neuron*, *8*(1), 3–11. https://doi.org/10.1016/0896-6273(92)90104-L

Calabrese, V., Mancuso, C., Calvani, M., Rizzarelli, E., Butterfield, D. A., & Giuffrida Stella, A. M. (2007). Nitric oxide in the central nervous system: Neuroprotection versus neurotoxicity. *Nature Reviews Neuroscience*, *8*(10), 766–775. https://doi.org/10.1038/nrn2214

Capaday, C. (2004). The integrative nature of motor cortical function. *The Neuroscientist*, *10*, 207–220.

Cauli, B., & Hamel, E. (2010). Revisiting the role of neurons in neurovascular coupling. *Frontiers in Neuroenergetics*, *2*, 9. https://doi.org/10.3389/fnene.2010.00009

Chapin, J. K., Moxon, K. A., Markowitz, R. S., & Nicolelis, M. A. (1999). Real-time control of a robotic arm using simultaneously recorded neurons in the motor cortex. *Nature Neuroscience*, *2*(7), 664–670.

Chen, T.-W., Wardill, T. J., Sun, Y., Pulver, S. R., Renninger, S. L., Baohan, A., Schreiter, E. R., Kerr, R. A., Orger, M. B., Jayaraman, V., Looger, L. L., Svoboda, K., & Kim, D. S. (2013). Ultrasensitive fluorescent proteins for imaging neuronal activity. *Nature*, *499*(7458), 295–300. https://doi.org/10.1038/nature12354

Clancy, B., Defelipe, J., Espinosa, A., Fairén, A., Jinno, S., Kanold, P., Heiko, J., Luhmann, H. J., Rockland, K. S., Tamamaki, N., & Yan, X. X. (2010). Cortical GABAergic neurons: Stretching it remarks, main conclusions and discussion. *Frontiers in Neuroanatomy*, *4*, 7. https://doi.org/10.3389/neuro.05.007.2010

Dawson, T. M., Bredt, D. S., Fotuhi, M., Hwang, P. M., & Snyder, S. H. (1991). Nitric oxide synthase and neuronal NADPH diaphorase are identical in brain and peripheral tissues. *Proceedings of the National Academy of Sciences of the United States of America*, *88*(17), 7797–7801. https://doi.org/10.1073/pnas.88.17.7797

Dawson, T. M., Zhang, J., Dawson, V. L., & Snyder, S. H. (1994). Nitric oxide: Cellular regulation and neuronal injury. In *Progress in brain research* (Vol. 103, pp. 365–369). Elsevier. https://doi.org/10.1016/S0079-6123(08)61150-4

Donoghue, J. P., Suner, S., & Sanes, J. N. (1990). Dynamic organization of primary motor cortex output to target muscles in adult rats II. Rapid reorganization following motor nerve lesions. *Experimental Brain Research*, *79*(3), 492–503. https://doi.org/10.1007/BF00229319

Donoghue, J. P., & Wise, S. P. (1982). The motor cortex of the rat: Cytoarchitecture and microstimulation mapping. *The Journal of Comparative Neurology*, *212*(1), 76–88. https://doi.org/10.1002/cne.902120106

Elston, G. N. (2002). Cortical heterogeneity: Implications for visual processing and polysensory integration. *Journal of Neurocytology*, *31*, 317–335. https://doi.org/10.1023/A:1024182228103

Elston, G. N., Elston, A., Freire, M. A. M., Gomes Leal, W., Dias, I. A., Pereira, A., Silveira, L. C. L., & Picanço Diniz, C. W. (2006). Specialization of pyramidal cell structure in the visual areas V1, V2 and V3 of the South American rodent, Dasyprocta primnolopha. *Brain Research*, *1106*(1), 99–110. https://doi.org/10.1016/j.brainres.2006.05.100

Ethier, C., Brizzi, L., Darling, W. G., & Capaday, C. (2006). Linear summation of cat motor cortex outputs. *The Journal of Neuroscience*, *26*(20), 5574–5581.

Franca, J. G., Volchan, E., Jain, N., Catania, K. C., Oliveira, R. L., Hess, F. F., Jablonka, M., Rocha-Miranda, C. E., & Kaas, J. H. (2000). Distribution of NADPH-diaphorase cells in visual and somatosensory cortex in four mammalian species. *Brain Research*, *864*(2), 163–175. https://doi.org/10.1016/S0006-8993(00)02058-8

Freire, M. A. M., Faber, J., Picanço-Diniz, C. W., Franca, J. G., & Pereira, A. (2012). Morphometric variability of nicotinamide adenine dinucleotide phosphate diaphorase neurons in the primary sensory areas of the rat. *Neuroscience*, *205*, 140–153. https://doi.org/10.1016/j.neuroscience.2011.12.029

Freire, M. A. M., Gomes-Leal, W., Carvalho, W. A., Guimarães, J. S., Franca, J. G., Picanço-Diniz, C. W., & Pereira, A. (2004). A morphometric study of the progressive changes on NADPH diaphorase activity in the developing rat's barrel field. *Neuroscience Research*, *50*(1), 55–66. https://doi.org/10.1016/j.neures.2004.05.009

Gabbott, P. L. A., & Bacon, S. J. (1995). Co-localisation of NADPH diaphorase activity and GABA immunoreactivity in local circuit neurones in the medial prefrontal cortex (mPFC) of the rat. *Brain Research*, *699*, 321–328.

Gao, P., Hattox, A. M., Jones, L. M., Keller, A., & Zeigler, H. P. (2003). Whisker motor cortex ablation and whisker movement patterns. *Somatosensory & Motor Research*, *20*, 191–198.

Garbossa, D., Fontanella, M., Tomasi, S., Ducati, A., & Vercelli, A. (2005). Differential distribution of NADPH-diaphorase histochemistry in human cerebral cortex. *Brain Research*, *1034*(1–2), 1–10. https://doi.org/10.1016/j.brainres.2004.10.049

Garthwaite, J. (2008). Concepts of neural nitric oxide-mediated transmission. *European Journal of Neuroscience*, *27*(11), 2783–2802. https://doi.org/10.1111/j.1460-9568.2008.06285.x

Garthwaite, J., & Boulton, C. L. (1995). Nitric oxide signaling in the central nervous system. *Annual Review of Physiology*, *57*, 683–706.

Graziano, M. S. A., Taylor, C. S. R., Moore, T., & Cooke, D. F. (2002). The cortical control of movement revisited. *Neuron*, *36*, 349–362.

Gundersen, H. J. G., Bendtsen, T. F., Korbo, L., Marcussen, N., Moller, A., Nielsen, K., Nyengaard, J. R., Pakkenberg, B., Sørensen, F. B., Vesterby, A., & West, M. J. (1988). Some new, simple and efficient stereological methods and their use in pathological research and diagnosis. *APMIS*, *96*, 379–394. https://doi.org/10.1111/j.1699-0463.1988.tb05320.x

Hall, R. D., & Lindholm, E. P. (1974). Organization of motor and somatosensory neocortex in the albino rat. *Brain Research*, *66*(1), 23–38. https://doi.org/10.1016/0006-8993(74)90076-6

Haselden, W. D., Kedarasetti, R. T., & Drew, P. J. (2020). Spatial and temporal patterns of nitric oxide diffusion and degradation drive emergent cerebrovascular dynamics. *PLoS Computational Biology*, *16*, e1008069. https://doi.org/10.1371/journal.pcbi.1008069

Hilbig, H., & Punkt, K. (1997). 24-hour rhythmicity of NADPH-diaphorase activity in the neuropil of rat visual cortex. *Brain Research Bulletin*, *43*(3), 337–340. https://doi.org/10.1016/S0361-9230(97)00016-6

Huh, Y., Lee, W., Cho, J., & Ahn, H. (1998). Regional changes of NADPH-diaphorase and neuropeptide Y neurons in the cerebral cortex of aged Fischer 344 rats. *Neuroscience Letters*, *247*, 79–82. https://doi.org/10.1016/S0304-3940(98)00240-7

Kubota, Y., Shigematsu, N., Karube, F., Sekigawa, A., Kato, S., Yamaguchi, N., Hirai, Y., Morishima, M., & Kawaguchi, Y. (2011). Selective coexpression of multiple chemical markers defines discrete populations of neocortical GABAergic neurons. *Cerebral Cortex*, *21*, 1803–1817. https://doi.org/10.1093/cercor/bhq252

Lindauer, U., Megow, D., Matsuda, H., & Dirnagl, U. (1999). Nitric oxide: A modulator, but not a mediator, of neurovascular coupling in rat somatosensory cortex. *Heart and Circulatory Physiology*, *277*, 799–811. https://doi.org/10.1152/ajpheart.1999.277.2.H799

Lübke, J., & Feldmeyer, D. (2007). Excitatory signal flow and connectivity in a cortical column: Focus on barrel cortex. *Brain Structure and Function*, *212*(1), 3–17. https://doi.org/10.1007/s00429-007-0144-2

Lüth, H.-J., Hedlich, A., Hilbig, H., Winkelmann, E., & Mayer, B. (1994). Morphological analyses of NADPH-diaphorase/nitric oxide synthase positive structures in human visual cortex. *Journal of Neurocytology*, *23*(12), 770–782. https://doi.org/10.1007/BF01268089

Matsumoto, T., Nakane, M., Pollock, J. S., Kuk, J. E., & Förstermann, U. (1993). A correlation between soluble brain nitric oxide synthase and NADPH-diaphorase activity is only seen after exposure of the tissue to fixative. *Neuroscience Letters*, *155*, 61–64. https://doi.org/10.1016/0304-3940(93)90673-9

Moncada, S., Palmer, R. M., & Higgs, E. A. (1991). Nitric oxide: Physiology, pathophysiology, and pharmacology. *Pharmacological Reviews*, *43*(2), 109–142.

Morandell, K., & Huber, D. (2017). The role of forelimb motor cortex areas in goal directed action in mice. *Scientific Reports*, *7*, 15759. https://doi.org/10.1038/s41598-017-15835-2

Nogueira-Campos, A. A., Finamore, D. M., Imbiriba, L. A., Houzel, J. C., & Franca, J. G. (2012). Distribution and morphology of nitrergic neurons across functional domains of the rat primary somatosensory cortex. *Frontiers in Neural Circuits*, *6*, 57. https://doi.org/10.3389/fncir.2012.00057

Paxinos, G., & Watson, C. (1997). The rat brain in stereotaxic coordinates, 3rd ed. *Journal of Anatomy*, *191*(2), 315–317. https://doi.org/10.1046/j.1469-7580.1997.191203153.x

Pchitskaya, E., & Bezprozvanny Ilya, K. (2020). Dendritic spines shape analysis. Classification or clusterization? *Frontiers in Synaptic Neuroscience*, *12*, 31. https://doi.org/10.3389/fnsyn.2020.00031

Petersen, C. C. H. (2007). The functional organization of the barrel cortex. *Neuron*, *56*(2), 339–355. https://doi.org/10.1016/j.neuron.2007.09.017

Romanelli, P., di Matteo, L., Cobellis, G., Varriale, B., Menegazzi, M., Gironi Carnevale, U., Ruocco, L. A., & Sadile, A. G. (2007). Transcription factor expression, RNA synthesis and NADPH-diaphorase across the rat brain and exposure to spatial novelty. *Behavioural Brain Research*, *184*(1), 91–100. https://doi.org/10.1016/j.bbr.2007.06.021

Sandell, J. H. (1986). NADPH diaphorase histochemistry in the macaque striate cortex. *The Journal of Comparative Neurology*, *251*, 388–397.

Santiago, L. F., Rocha, E. G., Freire, M. A. M., Dias, I. A., Lent, R., Houzel, J. C., Picanço-Diniz, C. W., Pereira, A., Jr., & Franca, J. G.

(2007). The organizational variability of the rodent somatosensory cortex. *Reviews in the Neurosciences, 18*(3–4), 283–294. https://doi.org/10.1515/REVNEURO.2007.18.3-4.283

Scherer-Singler, U., Vincent, S. R., Kimura, H., & McGeer, E. G. (1983). Demonstration of a unique population of neurons with NADPH-diaphorase histochemistry. *Journal of Neuroscience Methods, 9*(3), 229–234. https://doi.org/10.1016/0165-0270(83)90085-7

Schubert, D., Kötter, R., & Staiger, J. F. (2007). Mapping functional connectivity in barrel-related columns reveals layer- and cell type-specific microcircuits. *Brain Structure and Function, 212*(2), 107–119. https://doi.org/10.1007/s00429-007-0147-z

Schüz, A., & Palm, G. (1989). Density of neurons and synapses in the cerebral cortex of the mouse. *Journal of Comparative Neurology, 286*(4), 442–455. https://doi.org/10.1002/cne.902860404

Serruya, M. D., Hatsopoulos, N. G., Paninski, L., Fellows, M. R., & Donoghue, J. P. (2002). Instant neural control of a movement signal. *Nature, 416*, 141–142.

Stuehr, D. J. (2004). Enzymes of the L-arginine to nitric oxide pathway. *The Journal of Nutrition, 134*(10), 2748S–2751S. https://doi.org/10.1093/jn/134.10.2748S

Tandon, S., Kambi, N., & Jain, N. (2007). Overlapping representations of the neck and whiskers in the rat motor cortex revealed by mapping at different anaesthetic depths. *European Journal of Neuroscience, 27*(1), 228–237. https://doi.org/10.1111/j.1460-9568.2007.05997.x

Torres, J. B., Assunção, J., Farias, J. A., Kahwage, R., Lins, N., Passos, A., Quintairos, A., Trévia, N., & Diniz, C. W. P. (2006). NADPH-diaphorase histochemical changes in the hippocampus, cerebellum and striatum are correlated with different modalities of exercise and watermaze performances. *Experimental Brain Research, 175*(2), 292–304. https://doi.org/10.1007/s00221-006-0549-9

Vlasenko, O. V., Maisky, V. A., Maznychenko, A. V., & Pilyavskii, A. I. (2008). NADPH-diaphorase activity and neurovascular coupling in the rat cerebral cortex. *Fiziolohichnyĭ Zhurnal, 54*, 45–53.

Wallace, M. N. (1987). Histochemical demonstration of sensory maps in the rat and mouse cerebral cortex. *Brain Research, 418*(1), 178–182. https://doi.org/10.1016/0006-8993(87)90977-2

Wässle, H., & Boycott, B. B. (1991). Functional architecture of the mammalian retina. *Physiological Reviews, 71*(2), 447–480. https://doi.org/10.1152/physrev.1991.71.2.447

Wessberg, J., Stambaugh, C. R., Kralik, J. D., Beck, P. D., Laubach, M., Chapin, J. K., Kim, J., Biggs, S. J., Srinivasan, M. A., & Nicolelis, M. A. (2000). Real-time prediction of hand trajectory by ensembles of cortical neurons in primates. *Nature, 408*, 361–365.

Wester, J. C., & Contreras, D. (2012). Columnar interactions determine horizontal propagation of recurrent network activity in neocortex. *Journal of Neuroscience, 32*(16), 5454–5471. https://doi.org/10.1523/JNEUROSCI.5006-11.2012

Wolpaw, J. R. (2007). Brain-computer interfaces as new brain output pathways. *The Journal of Physiology, 579*, 613–619.

Wong-Riley, M., Anderson, B., Liebl, W., & Huang, Z. (1998). Neurochemical organization of the macaque striate cortex: Correlation of cytochrome oxidase with Na+K+ATPase, NADPH-diaphorase, nitric oxide synthase, and N-methyl-d-aspartate receptor subunit 1. *Neuroscience, 83*(4), 1025–1045. https://doi.org/10.1016/S0306-4522(97)00432-6

Wong-Riley, M. T., & Welt, C. (1980). Histochemical changes in cytochrome oxidase of cortical barrels after vibrissal removal in neonatal and adult mice. *Proceedings of the National Academy of Sciences of the United States of America, 77*(4), 2333–2337. https://doi.org/10.1073/pnas.77.4.2333

Yan, X. X., & Garey, L. J. (1997). Morphological diversity of nitric oxide synthesising neurons in mammalian cerebral cortex. *Journal für Hirnforschung, 38*(2), 165–172.

Yan, X. X., Jen, L. S., & Garey, L. J. (1996). NADPH-diaphorase-positive neurons in primate cerebral cortex colocalize with GABA and calcium-binding proteins. *Cerebral Cortex, 6*, 524–529. https://doi.org/10.1093/cercor/6.3.524

Zilles, K. (1985). *The cortex of the rat.* Springer. https://doi.org/10.1007/978-3-642-70573-1